


## Article

# Centennial Impacts of the East Asian Summer Monsoon on Holocene Deltaic Evolution of the Huanghe River, China

Yanping Chen <sup>1</sup>, Wenzhe Lyu <sup>2</sup>, Tengfei Fu <sup>2</sup>, Yan Li <sup>3</sup> and Liang Yi <sup>4,\*</sup> 

<sup>1</sup> Key Laboratory of Engineering Oceanography, Second Institute of Oceanography, Ministry of Natural Resources, Hangzhou 310012, China; chenai0812@163.com

<sup>2</sup> Key Laboratory of Marine Geology and Metallogeny, First Institute of Oceanography, Ministry of Natural Resources, Qingdao 266062, China; lvwenzhe1992@gmail.com (W.L.); futengfei@fio.org.cn (T.F.)

<sup>3</sup> School of Ocean Sciences, China University of Geosciences, Beijing 100083, China; geo-liyan@foxmail.com

<sup>4</sup> State Key Laboratory of Marine Geology, Tongji University, Shanghai 200092, China

\* Correspondence: yiliang@tongji.edu.cn

**Abstract:** The Huanghe River (Yellow River) is the most sediment laden river system in the world, and many efforts have been conducted to understand modern deltaic evolution in response to anthropological impacts. However, the natural background and its linkage to climatic changes are less documented in previous studies. In this work, we studied the sediments of core YDZ-3 and marine surface samples by grain-size analysis to retrieve Holocene dynamics of the Huanghe River delta in detail. The main findings are as follows: The mean value of sediment grain size of the studied core is  $5.5 \pm 0.9 \Phi$ , and silt and sand contents are  $5.2 \pm 2.3\%$  and  $8.2 \pm 5.3\%$ , respectively, while the variance of clay particles is relatively large with an average value of  $86.4 \pm 8.5\%$ . All grain-size data can be mathematically partitioned by a Weibull-based function formula, and three subgroups were identified with modal sizes of  $61.1 \pm 28.9 \mu\text{m}$ ,  $30.0 \pm 23.9 \mu\text{m}$ , and  $2.8 \pm 1.6 \mu\text{m}$ , respectively. There are eight intervals with abrupt changes in modal size of core YDZ-3, which can be correlated to paleo-superlobe migration of the Huanghe River in the Holocene. Based on these observations, the presence of seven superlobes in the history are confirmed for the first time and their ages are well constrained in this study, including Paleo-Superlobes Lijin (6400–5280 yr BP), Huanghua (4480–4190 yr BP), Jugezhuang (3880–3660 yr BP), Shajinzi (3070–2870 yr BP), Nigu (2780–2360 yr BP), Qikou (2140–2000 yr BP), and Kenli (1940–1780 and 1700–1650 yr BP). By tuning geomorphological events to a sedimentary proxy derived from core YDZ-3 and comparing to various paleoenvironmental changes, we proposed that winter climate dominated Holocene shifts of the Huanghe River delta on millennial timescales, while summer monsoons controlled deltaic evolution on centennial timescales.

**Keywords:** Huanghe River (Yellow River); paleo-superlobes; deltaic evolution; Asian monsoon; the Holocene; sediment grain size; centennial timescales



**Citation:** Chen, Y.; Lyu, W.; Fu, T.; Li, Y.; Yi, L. Centennial Impacts of the East Asian Summer Monsoon on Holocene Deltaic Evolution of the Huanghe River, China. *Appl. Sci.* **2021**, *11*, 2799. <https://doi.org/10.3390/app11062799>

Academic Editors:  
Edoardo Rotigliano and Marta  
Pérez Arlucea

Received: 12 January 2021

Accepted: 18 March 2021

Published: 21 March 2021

**Publisher's Note:** MDPI stays neutral with regard to jurisdictional claims in published maps and institutional affiliations.



**Copyright:** © 2021 by the authors. Licensee MDPI, Basel, Switzerland. This article is an open access article distributed under the terms and conditions of the Creative Commons Attribution (CC BY) license (<https://creativecommons.org/licenses/by/4.0/>).

## 1. Introduction

The Huanghe River (Yellow River) is the second-longest river in China, and the fifth-longest and the most sediment laden river in the world. The river originates from the northeastern part of the Tibetan Plateau, flows across the Chinese Loess Plateau, and discharges into the western Bohai Sea (Figure 1). The annual sediment loads of the Huanghe River are  $\sim 1.08 \times 10^9$  tons [1], and most recently, anthropological impacts on sediment supply of the Huanghe River have become profound [2,3]. For example, the delta of the Huanghe River stands at the threshold between erosion and aggradation, according to the fluvial discharge rate of  $7.67 \times 10^9 \text{ m}^3/\text{year}$  and the sediment load of  $0.278 \times 10^9 \text{ ton/year}$  [4]. Since millions of people live on the delta, establishing the natural

background of the Huanghe River is critical to social and scientific issues, such as future policy, water-resource management, and coastal engineering [5–8].

During the early-Holocene transgression, sedimentary environments along the coastal areas of the Bohai Sea changed from rivers and lakes to tidal flats and estuaries [9,10], and the paleo-environment shifted to a deltaic one at ~6000  $^{14}\text{C}$  yr BP [8,10]. Subsequently, 10 paleo-superlobes (PSLs) of the Huanghe River were developed, nine of them on the western coast of the Bohai Sea, and the other on the western coast of the Huanghai Sea (Yellow Sea) during 1128–1855 AD [10,11]. The Yangtze River delta was affected by the Yellow River when it shifted to the Huanghai Sea [12], and the present Yellow River delta, referred to PSL-10, formed after an artificial river-course shift in 1855 AD, from the Huanghai Sea back to the Bohai Sea (Figure 1).

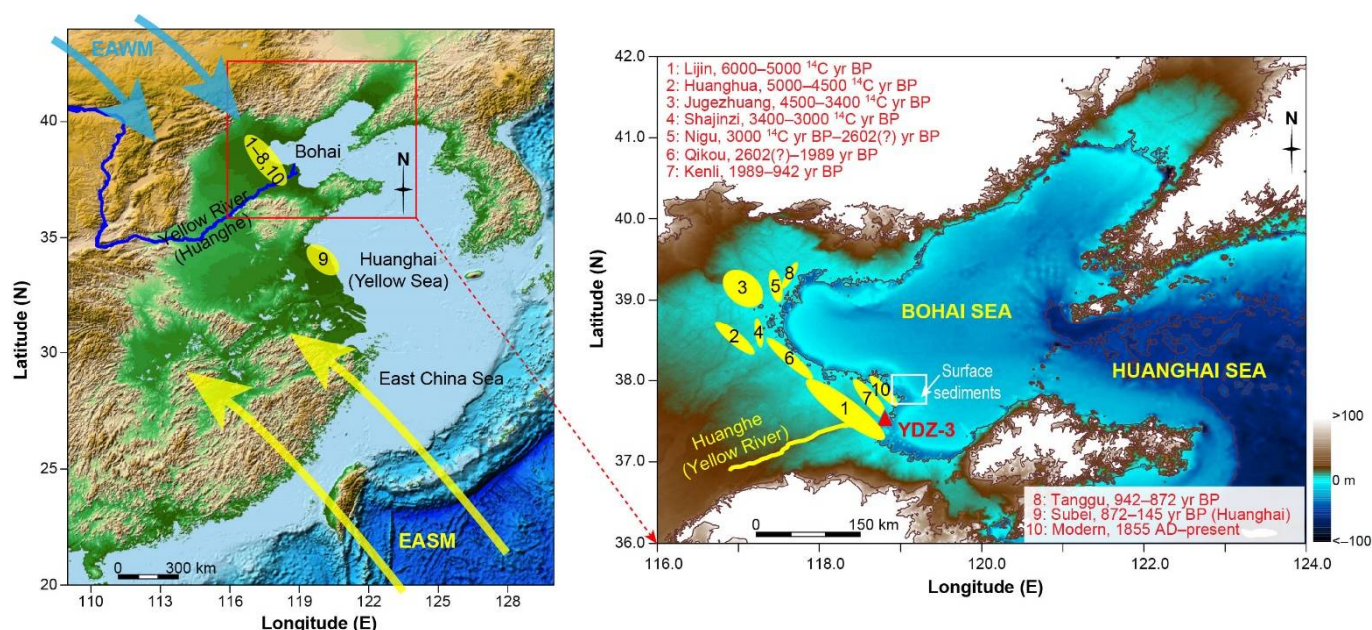


**Figure 1.** Study area, paleo-superlobes [10,11,13], and YDZ-3 location. The ten paleo-superlobes of the Yellow River delta in the Holocene are labeled as numbers. Marine surface sediments in the Yellow River estuary [14] were analyzed for reference. EASM, East Asian summer monsoon; EAWM, East Asian winter monsoon. The base map data was generated using the open and free software DIVA-GIS 7.5 (<http://www.diva-gis.org/>, accessed on 20 March 2021).

Holocene and recent changes of the Huanghe River are characterized by large sediment loads and frequent shifts of terminal channel [1,11]. It was reported that the Huanghe River runoff and sediment loads were dominated by the East Asian summer monsoon (EASM), and over the past 500 years, either runoff or sediment loads have been unprecedented due to human activities [6]. Based on shelly ridges of the west coast of the Bohai Sea, it is inferred that there were ten periods for the PSL development since the middle Holocene [15]. By radiocarbon dating of shell fossils, organic carbon without calibration, or historical documents about the Huanghe River rechanneling, PSL-1, -6, -7 have been confirmed by regional sequence stratigraphy [10,11,13]; however, other PSLs are not well constrained. Typically, deltas usually contain several superlobes, which develop at river mouths in response to regional sea level changes, such as transgressive and regressive phases [16] and sediment accumulation rate [17]. Superlobes initiate in the case of a shift in the river's terminal channel when the lower reaches were overloaded [13], resulting in abandoning the old channel, leading to evulsion, and developing/invading a new terminal channel. Thus, there should be a close linkage between climate changes and deltaic evolution.

Controlling factors of the Yellow River delta are somehow conflicted, since different seasons were highlighted in various studies, in which shortcomings are evident. For example, the one highlighting factors in summers only covered two PSL shifts [6], while the one

proposing winter factors on millennial timescales missed two PSL shifts [8]. Understanding the mechanism of deltaic evolution is very important not only in the Huanghe River [18], but also in other mega-deltas, such as those of the Nile, Mississippi, and Mekong [2,19,20]. In previous studies, deltaic evolution was usually reconstructed from a lithological and geomorphological perspective [21–24], and comparisons on centennial, millennial, or orbital timescales are less conducted. In this study, we analyze sediment grain-size data of a core from the southern Yellow River delta and discuss the distinct roles of the EASM and the Asian winter monsoon (EAWM) on different timescales.

## 2. Materials and Methods

### 2.1. Core YDZ-3

Core YDZ-3 was drilled on the southern part of the Huanghe River delta (37°27' N, 118°55' E) by the East China Normal University in 2009, using a vertical drilling rig. The drilling site was underwater until the end of the twentieth century. The length of the core is 34.7 m with a recovery rate of 91% (Figure 2). Seven peat samples from 7.7–18.0 m depth interval were well constrained by radiocarbon dating, and the age model was established based on a second-order polynomial fit, taking into account the 95.4% confidence intervals [8].

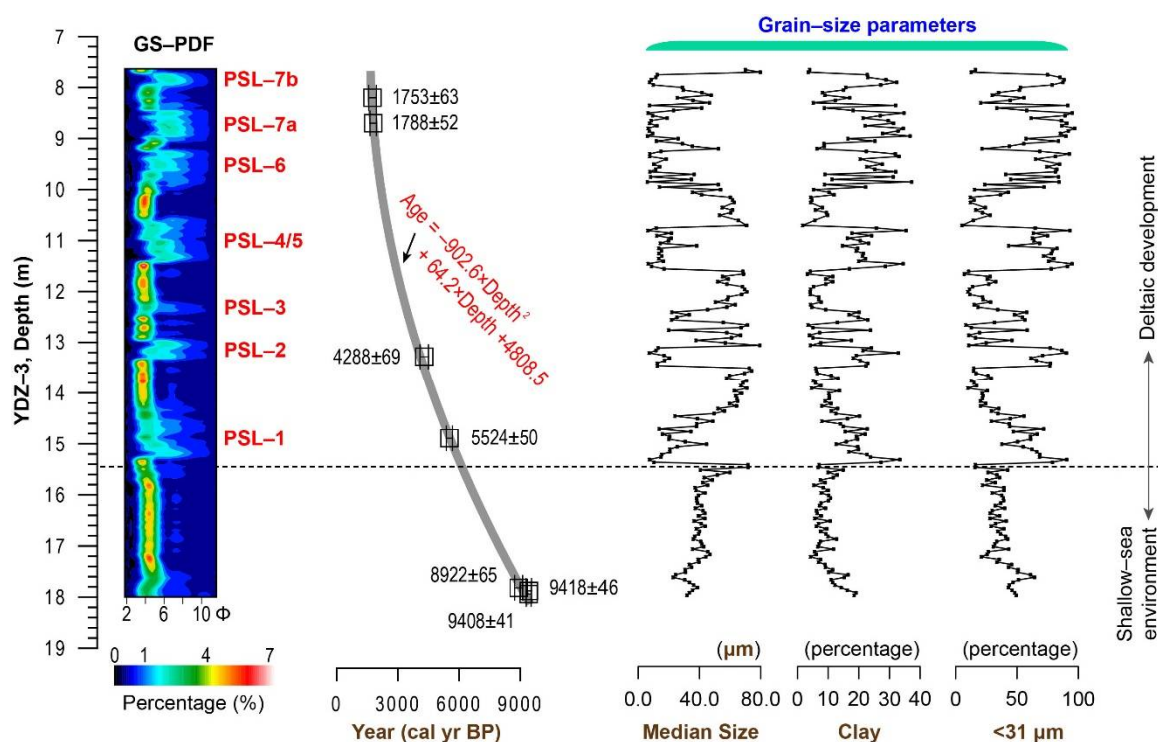


**Figure 2.** GS-PDF, age model, median size, clay component, and the content of grain-size < 31 μm of core YDZ-3. GS, sediment grain size; PDF, probability density function of sediment grain-size spectrum; PSL, paleo-superlobe.

### 2.2. Grain-Size Measurement

A total of 203 grain-size samples were collected from 7.7–18.0 m depth interval of the core and 35 samples of marine surface sediments were measured for reference (Figure 1). The grain size samples were pretreated with 10–20 mL of 30% H<sub>2</sub>O<sub>2</sub> to remove organic matter, washed with 10% HCl to remove carbonates, rinsed with deionized water, and then placed in an ultrasonic bath for several minutes to facilitate dispersion. The grain size spectra of the remaining terrigenous material were measured using a Malvern Mastersizer 2000 laser-particle size analyzer at Second Institute of Oceanography, Ministry of Natural Resources of China. One hundred grain size classes between 0.3 and 300 μm were exported for further analysis.

### 2.3. Unmixing Grain-Size Distribution

Mathematical methods have been introduced to define all types of sediment grain-size distributions and to partition grain-size components of poly-modal sediments with grain-size data generated by laser analyzers [25–30], which can reveal much more details than using grain-size analysis of bulk samples. It can be mathematically proven that a poly-modal distribution of bulk samples can be expressed as [31]:

$$f = p_1 f_1 + p_2 f_2 + \dots + (1 - p_1 - p_2 - \dots - p_{n-1}) f_n \quad (1)$$

where  $f_i$  represents the prototype function of component  $i$  with a total number of  $n$ , and  $p_i$  is its percentage in the bulk sample. There are  $n - 1$  coefficients,  $p_i$ , to be estimated due to the sum of percentages equaling unity.

Since partitioning of sediment grain-size spectrum by a Weibull distribution is robust and has broad applicability, relative to Normal,  $t$ ,  $F$ ,  $\chi^2$ , and  $\gamma$  distributions [30], we chose the Weibull as the common pattern in this study. The Weibull distribution can be skewed in either direction or even made symmetric by designating specific parameters, and its prototype formula is as follows:

$$f(x, \alpha, \beta) = \frac{\alpha}{\beta^\alpha} x^{\alpha-1} e^{-(\frac{x}{\beta})^\alpha} \quad (2)$$

The  $\alpha$  determines the distribution's shape, including the skewness and symmetry of the curve,  $\beta$  controls the position of the primary frequency of the curve, here referred to as the position of the modal grain size, and  $x$  is a variable representing grain size.

## 3. Results

### 3.1. Grain-Size Properties

Throughout the studied interval of core YDZ-3 (7.7–18.0 m), the mean value of sediment grain size ( $M_z$ ) is  $5.5 \pm 0.9 \Phi$ , which indicates a relatively high-dynamic sedimentary processes that changed significantly in the Holocene. The contents of silt ( $4\text{--}63 \mu\text{m}$ ) and sand ( $>63 \mu\text{m}$ ) particles are  $5.2 \pm 2.3\%$  and  $8.2 \pm 5.3\%$ , respectively, while the variance of clay particles ( $<4 \mu\text{m}$ ) is relatively large with an average value of  $86.4 \pm 8.5\%$  (Figure 2). To identify the characterized dynamic components, two parameters were selected:  $M$  value, the median diameter, indicating the mean hydrodynamic energy;  $C$  value, the one percentile of grain size distribution, representing the most hydrodynamic sedimentary component. The  $C$ – $M$  diagram can provide valuable insights into sediment transport and hydrodynamic intensity [32,33]. As shown, these two parameters were coupled (Figure 3b), and this relationship is also evident in marine surface sediments around the present Huanghe River mouth [14], the mud area of the Bohai Sea [34], the Laizhou Bay [35], and the abandoned Huanghe River mouth in the west of the Huanghai Sea [36]. Hence, it is inferred that the most dynamic component in core YDZ-3 was integrated into deltaic and estuary deposition with the mean state of various sedimentary processes.

For down-core variation, changes in sediment grain-size parameters can be generally grouped into two intervals (Figure 2): small fluctuation prior to  $\sim 6400$  yr BP and greater since then. In specific, prior to  $\sim 6400$  yr BP, all grain-size parameters were characterized by less variation without any distinct changes, and in contrast, since  $\sim 6400$  yr BP, these records varied greater. Eight episodes with a high clay content can be identified, namely 6400–5280 yr BP, 4480–4190 yr BP, 3880–3660 yr BP, 3070–2870 yr BP, 2780–2360 yr BP, 2140–2000 yr BP, 1940–1780 yr BP, and 1700–1650 yr BP. All of the alternations between these sub-stages were not stepwise but abrupt (Figure 2).



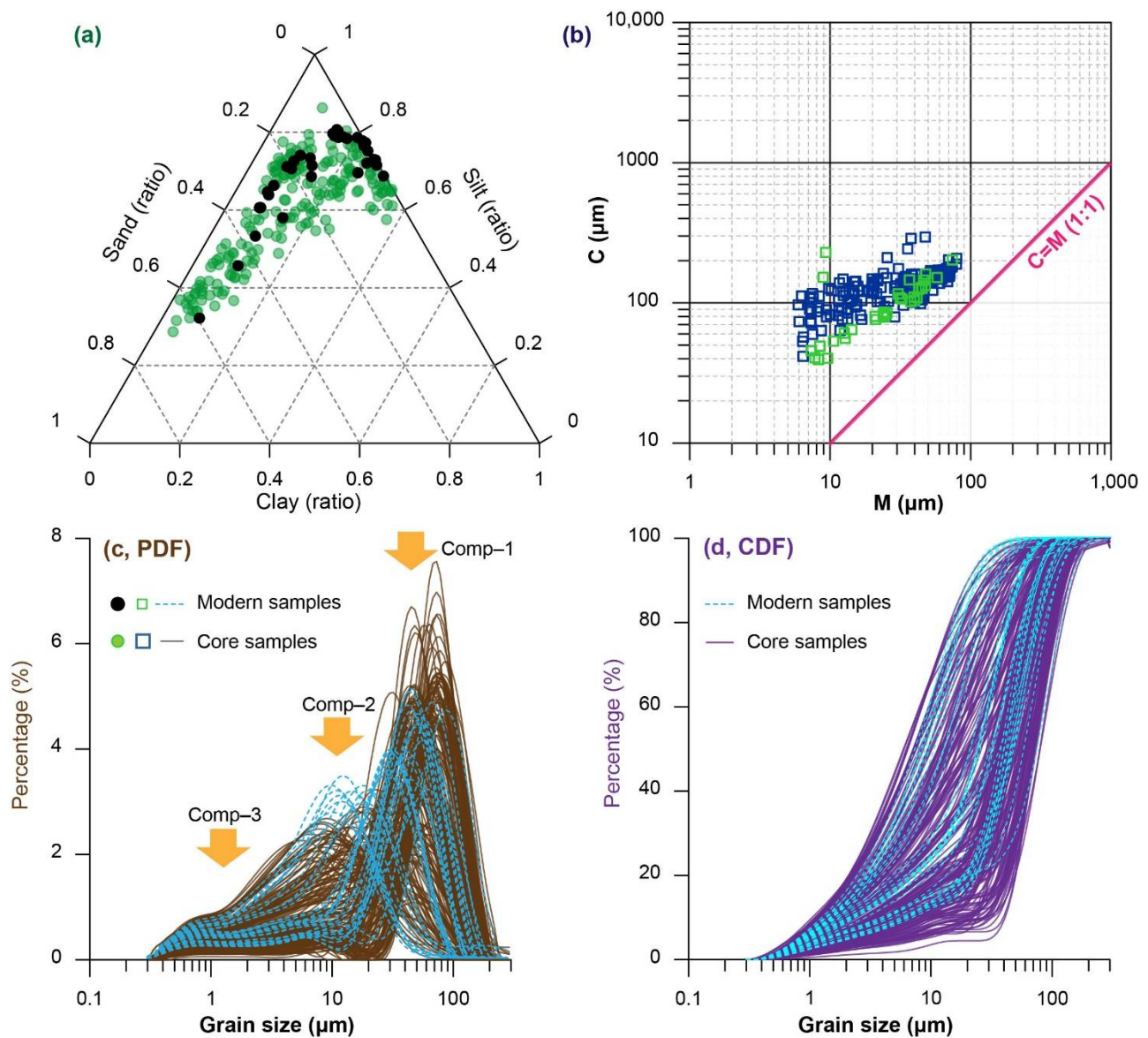


**Figure 3.** Characteristics of sediment grain size of core YDZ-3 and 35 surface samples. (a) Ternary diagrams; (b) C–M diagrams; (c,d) Grain-size distributions, PDF: probability density function, CDF: cumulative distribution function. Comp-1, -2, and -3 are three components by mathematical unmixing in Figure 4.

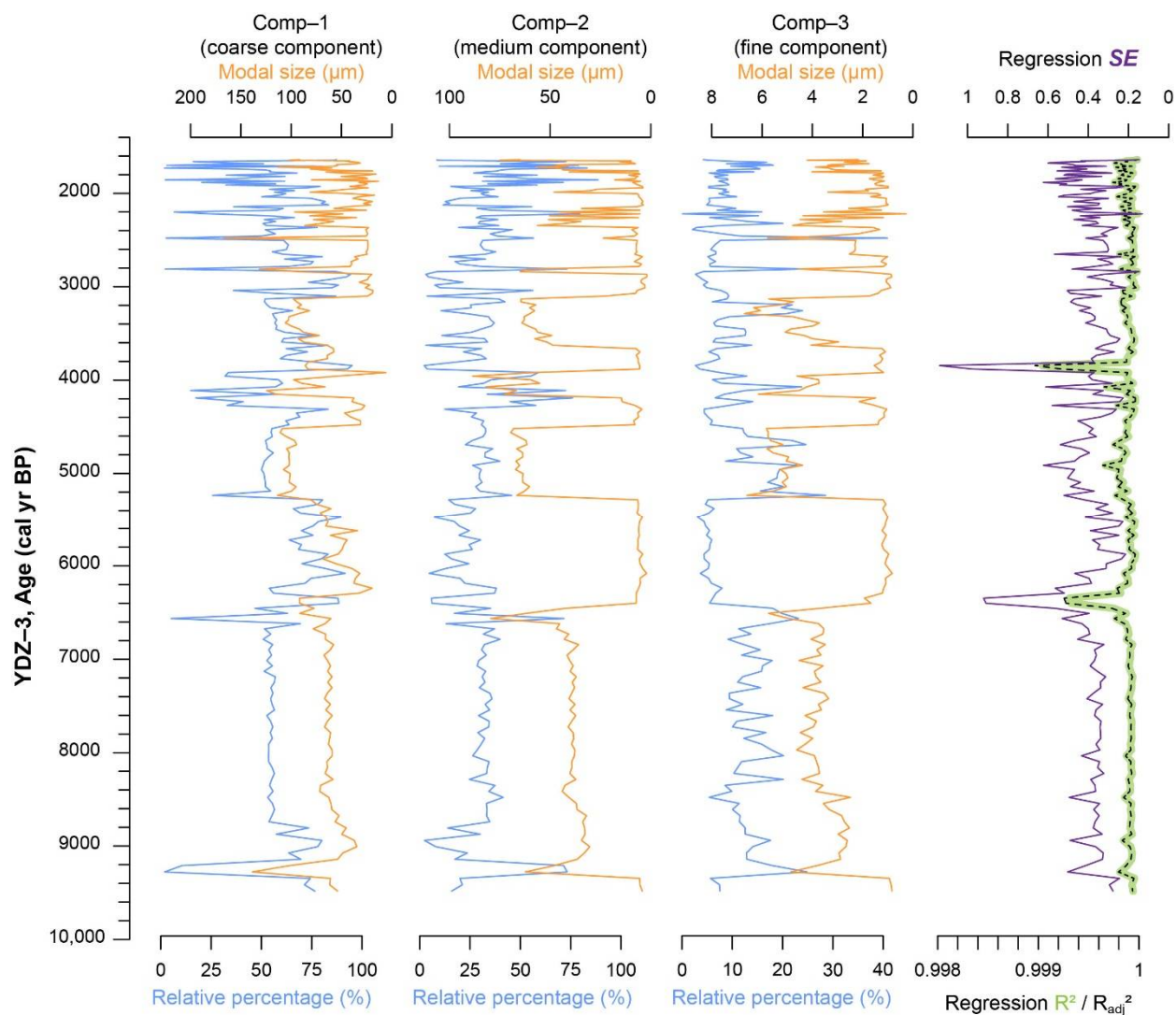


**Figure 4.** Down-core variation of unmixed components of core YDZ-3 with modes and contents. The right panel shows decomposition  $R^2$  (bold green line),  $R^2_{adj}$  (dashed black line), and standard error of the regression (SE) (thin purple line) were employed for helping choosing the best fit of partitioning estimations. Comp-1, -2, -3 are three components by unmixing.

### 3.2. Results of Grain-Size Unmixing

For grain-size distribution, a multi-mode pattern is observed, which agrees well with marine surface samples (Figure 3c). Because grain-size distribution of all samples consists of three components, the Weibull-based function formula for partitioning can be expressed as follows:

$$\begin{aligned}
 f(x, \alpha_1, \beta_1, m_1, \alpha_2, \beta_2, m_2, \alpha_3, \beta_3) &= m_1 \frac{\alpha_1}{\beta_1^{\alpha_1}} x^{\alpha_1-1} e^{-\left(\frac{x}{\beta_1}\right)^{\alpha_1}} + m_2 \frac{\alpha_2}{\beta_2^{\alpha_2}} x^{\alpha_2-1} e^{-\left(\frac{x}{\beta_2}\right)^{\alpha_2}} + (1 - m_1 \\
 &\quad - m_2) \frac{\alpha_3}{\beta_3^{\alpha_3}} x^{\alpha_3-1} e^{-\left(\frac{x}{\beta_3}\right)^{\alpha_3}}
 \end{aligned} \quad (3)$$

The values  $\alpha_1$  and  $\beta_1$  are parameters of the distribution function of the coarse-grained component,  $\alpha_2$  and  $\beta_2$  represent the medium-grained component, and  $\alpha_3$  and  $\beta_3$  are parameters of the fine-grained component. The percentages of each component in a sub-population are given by  $m_1$ ,  $m_2$ ,  $(1 - m_1 - m_2)$ , respectively. Here,  $x$  is a variable representing grain size.

Using the measured grain-size data from Malvern Mastersizer 2000 analyzer (MalvernPANalytical, Malvern, UK), i.e., one hundred grain-size classes between 0.3  $\mu\text{m}$  and 300  $\mu\text{m}$ , these eight parameters can be estimated following the General Least Square Fitting, setting the squared sum of the residual error to the minimum in multiple dimensions [37]. Three statistics, including R-squared ( $R^2$ ), adjusted R-squared ( $R^2_{\text{adj}}$ ), and standard error of the regression ( $SE$ ), were employed for choosing the best fit of estimations (Figure 4).

As a result, all samples have been well unmixed. Modal sizes of each component (labelled Comp-1, -2, -3) are  $61.1 \pm 28.9 \mu\text{m}$ ,  $30.0 \pm 23.9 \mu\text{m}$ , and  $2.8 \pm 1.6 \mu\text{m}$ , respectively, and their relative percentages are  $57.6 \pm 19.4\%$ ,  $32.0 \pm 17.0\%$ ,  $10.4 \pm 5.9\%$ , respectively. All regressions are significant in statistics, and  $R^2$  and  $R^2_{\text{adj}}$  are over 0.997 with  $SE$  of  $0.395 \pm 0.127$  (Figure 4), illustrating the reliability of unmixing processes.

Specifically, changes in modal sizes of each component are similar, while changes in contents are different (Figure 4). Prior to ~6400 yr BP, all parameters changed little, and after that, all changes were amplified, consistent with other grain-size parameters (Figure 2). Eight intervals can be similarly identified according to changes in modal sizes, and between each interval, all transitions are abrupt. A negative correlation between Comp-1 and Comp-2 contents is also evident. Integrating these findings, it is inferred that although modal sizes and contents of the three components are different, all parameters are closely correlated, indicating only one major factor controlling sedimentary dynamics of core YDZ-3 in the Holocene.

## 4. Discussion

### 4.1. Correlating Modal-Size Changes to Paleo-Superlobes Shifts

Typically, deltas can be classified as three types: river-, wave-, or tide-dominated systems [38], and most natural systems are developed between the three end members. This process can be simplified as that a river supplies clastic sediments to the receiving basin more rapidly than marine processes can remove it [8]. In this case, deltaic materials should increase abruptly when a delta starts, and similarly decrease when a superlobe migrates.

In the study area, the regional sea level rose up to the highest level at ~7000–6000 yr BP [39,40], and due to sea-level rise stagnation [17,41], the Huanghe River delta initiated at ~6000  $^{14}\text{C}$  yr BP [10,11,13]. Prior to construction of major river dams, the hydrodynamics involved in deltaic erosion were much less than sediment inputs, resulting in progradation of the delta [42–44]. Core YDZ-3 locates downstream to each PSL, and the drilling site was underwater prior to 1855 AD. Because the delta area is generally dominated by cyclonic tidal and geostrophic flows, the YDZ-3 site can record the major changes of the Huanghe River delta in the Holocene. Due to its distal position, the characterized variability of the unmixed grain-size components can be correlated to the eight intervals of changing channel and chenier development in the Holocene (Figure 5).

The basic linkage of this correlation can be summarized as follows: when a superlobe started, the amount of deposited materials increased suddenly, causing fine particles in the sediments to significantly and sharply increase; and in contrast, when a superlobe ceased, the amount of fine-grained materials decreased. Because Comp-2 is the component close to the marine surface sediments [14] and considering the relatively coarse-grained sediments in local rivers [45,46], the Comp-2 record of modal size and relative percentage was employed for later analysis.

Based on changes in Comp-2 modal size, the presence of all the seven PSLs are firstly confirmed in this study (Figure 5), namely 6400–5280 yr BP (PSL-1), 4480–4190 yr BP (PSL-2), 3880–3660 yr BP (PSL-3), 3070–2870 yr BP (PSL-4), 2780–2360 yr BP (PSL-5), 2140–2000 yr BP (PSL-6), and 1940–1780 and 1700–1650 yr BP (PSL-7). The timing of these intervals is close to the original proposal of PSLs [15], but with a clearer age limit for each PSL. Although the precise age of these intervals cannot be checked by a single core, the procedure for identifying PSLs in sedimentary sequences in this study may provide a valuable and effective way in future work.

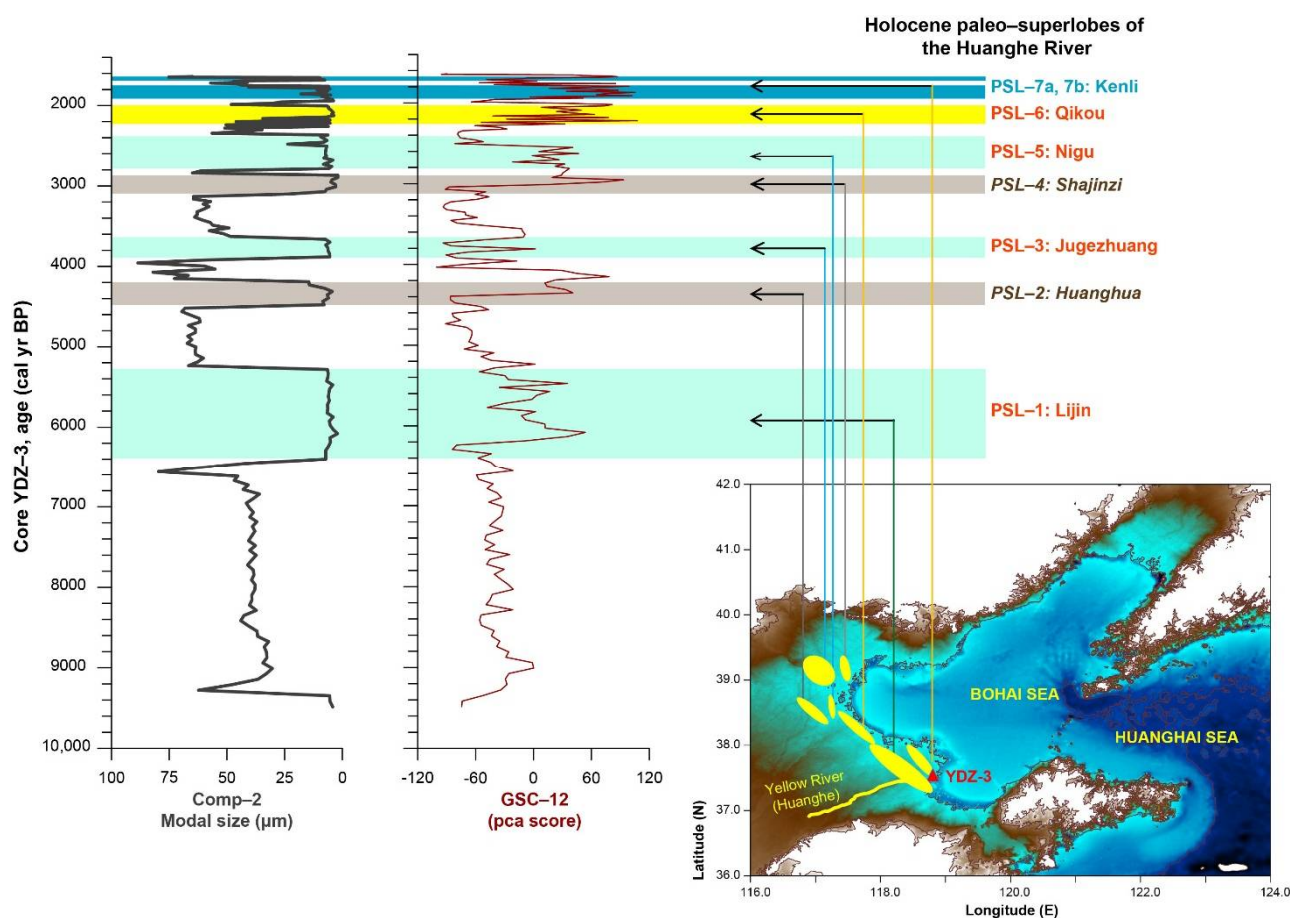


**Figure 5.** Correlating YDZ-3 comp-2 modal-size record to paleo-superlobe shifts of the Huanghe River and deriving forces of Holocene dynamics on millennial timescales. Seven PSLs (PSL-1 to –7) were labeled as in color bars, and two of them (PSL-2, PSL-4) were missed in the GSC-12 record [8].

Tuning geomorphological events to a well-dated and directly-linked proxy offers an opportunity to testify climatic influences on deltaic evolution of the Huanghe River on different timescales. The catchment of the Huanghe River is affected by the following climatic systems: (1) EASM carries moisture and induces sediment delivery; (2) Kuroshio Current (KC) modulates winter climate of eastern China; and (3) EAWM associated with the Bond ice-rafting debris (IRD) events dominates erosions in the catchment.

In winters, it has been proposed that the reduced cyclone frequency and dust storms in northern China could weaken erosion in the catchment and decrease sediment loads [8]. When sediment loads descend low enough, for example  $0.278 \times 10^9$  ton/year, a modern threshold [4], the delta lies close to a silting threshold. The silting threshold is critical, because below the value, river channels become self-adapting, interacting with floods, storm surges, or variations in tidal regime or wave action by enhanced channel erosion and greater potential for avulsion [47]. In this case, if sediment loads suddenly increase, the equilibrium will be disturbed, resulting in overloaded channels or channel avulsion. Considering that PSL shifts of the Huanghe River (Comp-2 modal size) are characterized by low-frequency variation (Figure 6a), the impacts of winter climates on deltaic evolution of the Huanghe River may be dominated on millennial timescales [8].

Moreover, based on the PCA result of sediment grain-size, Yi et al. [8] only identified five PSLs of the Huanghe River in sedimentary sequences but missed two PSLs (Figure 5), and they also claimed no consistency between deltaic evolution of the Huanghe River and EASM changes. Checking the difference between two methods, we found that the information of sedimentary dynamics (modal size) and relative contribution (content) are combined in the PCA result. This integration may cause centennial changes to not be



evident in the derived record (GSC-12). Hence, we suggest that in a complex sedimentary environment, such as the Huanghe River delta, multiple checks between different grain-size analyses are necessary.

#### 4.2. Influence of Summer Monsoon on Centennial Timescales

The Huanghe River flows across the Chinese Loess Plateau, and monsoonal climate is one of the most influential factors controlling this erosion [48,49]. Modern observations suggest that seasonal changes in water discharge and sediment loads of the Huanghe River were coupled [8], inferring that the massive amount of EASM rainfall plays an important role in sediment delivery and erosion [6]. Because the record of Comp-2 content is characterized by centennial variabilities (Figure 6b), we compared this record to the EASM in high-frequency bands (<500 yr).

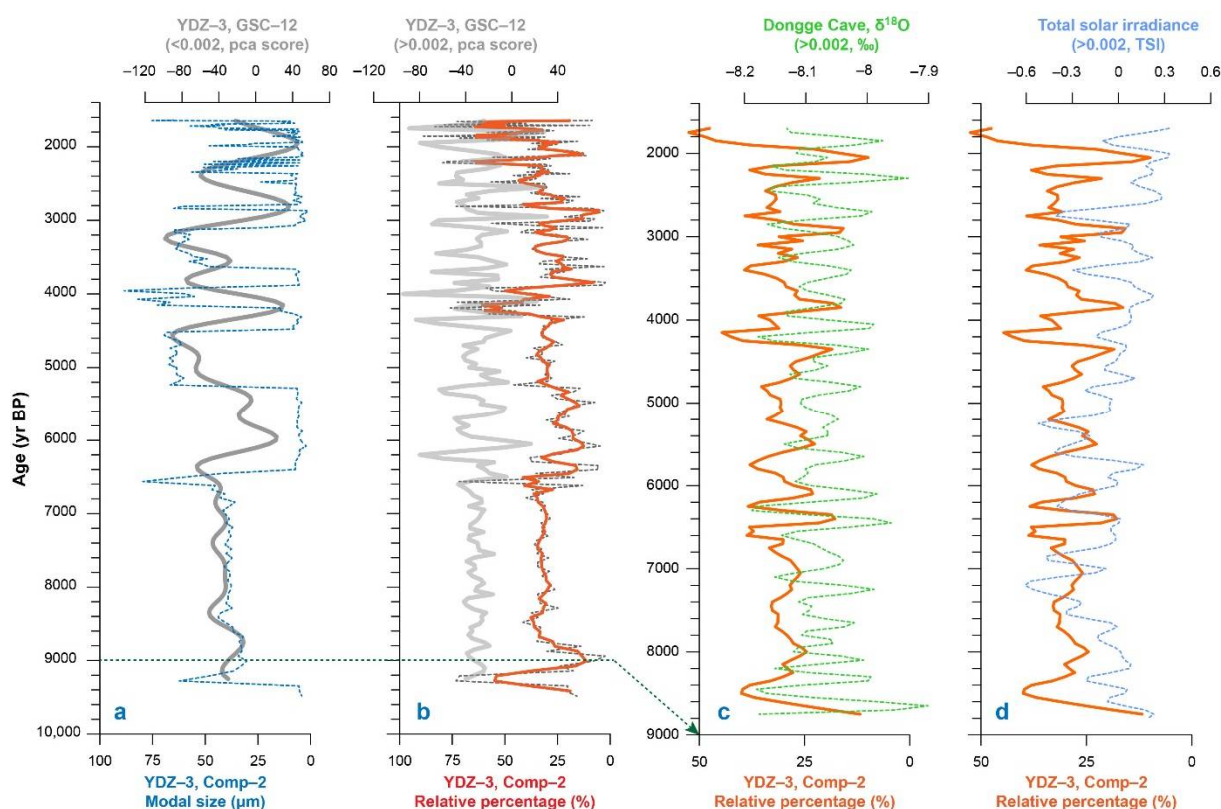


**Figure 6.** Correlating YDZ-3 record to various paleoenvironmental proxies on centennial timescales. (a) YDZ-3 Comp-2 modal size with the low-frequency (<0.002) component of GSC-12 record [8]; (b) YDZ-3 Comp-2 relative percentage (original value, dashed line; 3-point moving average, solid line) with the high-frequency (>0.002) component of GSC-12 record [8]; (c) Comparison between YDZ-3 Comp-2 relative percentage and the high-frequency (>0.002) component of Dongge Cave  $\delta^{18}\text{O}$  record [50]; (d) Comparison between YDZ-3 Comp-2 relative percentage and the high-frequency (>0.002) component of total solar irradiance (TSI) during the Holocene [51]. Noted that data in (c,d) are 3-point moving average records.

As shown, a good agreement was observed between YDZ-3 Comp-2 and EASM changes (Figure 6c), indicating summer climate is another important factor on centennial timescales, dominating deltaic evolution of the Huanghe River. The agreement may demonstrate that: (1) although erosion mainly occurs in winters, most of the eroded materials are carried by rivers in summers; and (2) monsoonal rainfall could enhance erosion in the catchment during flood periods. Thus, considering YDZ-3 location and the significant relationship between water discharge and regional precipitation [14], the linkage between deltaic evolution and EASM changes can be summarized as follows: When EASM strengthened, total rainfall across the catchments increased, and water discharge

and sediment loads enhanced, resulting in accelerating the progradation of the Huanghe River delta and/or overloaded channels.

Moreover, a number of paleoclimatic studies claimed that changes in solar irradiance influenced millennial-scale climates, such as the Bond IRD events [52], Asian monsoon [50,53], and KC [54], while no persistent phase association was reported between PSL shifts of the Huanghe River and solar activities [8]. Comparing total solar irradiance (TSI) with our proxies of deltaic evolution on centennial timescales, a direct correlation was observed (Figure 6d). Therefore, we proposed that solar activities could be an important factor dominating geomorphological evolution, such as deltaic development of the Huanghe River on centennial timescales via the effect of summer monsoon.

Integrating millennial and centennial impacts of Asian monsoon, the natural processes of Holocene delta of the Huanghe River can be identified. On the first order, winter climate over East Asia is the dominant factor in deltaic evolution, which induces erosions in the catchment on millennial timescales. On the second order, summer climate related to monsoonal changes is the dominant factor, which influences the transport of erosional materials to the delta on centennial timescales.

Since ~2360 yr BP, changes in sedimentary proxies of core YDZ-3 are amplified at a higher frequency (Figures 5 and 6), which could be correlated to the frequent channel shift of the Huanghe River [10,11,13]. It is thus inferred that the stability of the delta has decreased significantly, probably responding to the accelerating and strengthening impacts of human activities since the Warring States Period in Chinese history (~2400 yr BP). However, the shifts of PSLs 4–7 covaried generally with the millennial variabilities of sedimentary proxies of core YDZ-3 (Figure 6a), likely inferring that the anthropogenic impacts may be the major factor on the third order.

## 5. Conclusions

To document Holocene deltaic evolution of the Huanghe River, core YDZ-3 and marine surface sediments were studied in terms of sediment grain-size analysis, and paleo-superlobe migrations were tuned to sedimentary sequences. We found that the mean value of sediment grain size is  $5.5 \pm 0.9 \Phi$  in core YDZ-3, and silt and sand particles changed relatively little with average values of  $5.2 \pm 2.3\%$  and  $8.2 \pm 5.3\%$ , respectively, while clay content is  $86.4 \pm 8.5\%$ . To isolate different sedimentary processes, sediment grain-size spectrum was mathematically partitioned into three subgroups by a Weibull-based equation, and their modal sizes are  $61.1 \pm 28.9 \mu\text{m}$ ,  $30.0 \pm 23.9 \mu\text{m}$ , and  $2.8 \pm 1.6 \mu\text{m}$ , respectively. Based on these observations, eight intervals with abrupt changes in modal sizes were identified and then correlated to the seven paleo-superlobes of the Huanghe River in the Holocene. This correlation confirmed the presence of Paleo-superlobes Lijin (6400–5280 yr BP), Huanghua (4480–4190 yr BP), Jugezhuang (3880–3660 yr BP), Shajinzi (3070–2870 yr BP), Nigu (2780–2360 yr BP), Qikou (2140–2000 yr BP), and Kenli (1940–1780 and 1700–1650 yr BP) in the history. By tuning geomorphological events to the sedimentary proxy derived in this study, summer monsoon was proposed to be the major factor controlling deltaic evolution on centennial timescales. Therefore, we concluded that both summer and winter monsoons have played critical roles in deltaic evolution of the Huanghe River on different timescales and solar activities could be an important factor shaping geomorphological features in the Holocene.

**Author Contributions:** Conceptualization and methodology, L.Y.; formal analysis, Y.C., W.L., T.F. and Y.L.; original draft preparation, Y.C. and L.Y.; review and editing, Y.C., W.L., T.F. and Y.L. All authors have read and agreed to the published version of the manuscript.

**Funding:** This research was funded by the National Natural Science Foundation of China, grant numbers 41602349 and 41706068, the Natural Science Foundation of Shanghai, grant number 19ZR1459800, and the Beijing Natural Science Foundation, grant number 8204070.

**Institutional Review Board Statement:** Not applicable.

**Informed Consent Statement:** Not applicable.

**Data Availability Statement:** Data are available on request the corresponding author (yiliang@tongji.edu.cn).

**Acknowledgments:** We thank Chen, Shenliang in the East China Normal University for providing samples for this study.

**Conflicts of Interest:** The authors declare no conflict of interest.

## References

1. Milliman, J.D.; Syvitski, J.P.M. Geomorphic/Tectonic Control of Sediment Discharge to the Ocean: The Importance of Small Mountainous Rivers. *J. Geol.* **1992**, *100*, 525–544. [\[CrossRef\]](#)
2. Wang, H.; Saito, Y.; Zhang, Y.; Bi, N.; Sun, X.; Yang, Z. Recent changes of sediment flux to the western Pacific Ocean from major rivers in East and Southeast Asia. *Earth Sci. Rev.* **2011**, *108*, 80–100. [\[CrossRef\]](#)
3. Wang, H.; Yang, Z.; Saito, Y.; Liu, J.P.; Sun, X.; Wang, Y. Stepwise decreases of the Huanghe (Yellow River) sediment load (1950–2005): Impacts of climate change and human activities. *Glob. Planet. Chang.* **2007**, *57*, 331–354. [\[CrossRef\]](#)
4. Xu, J. A study of thresholds of runoff and sediment for the land accretion of the Yellow River Delta. *Geogr. Res.* **2002**, *21*, 163–170. [\[CrossRef\]](#)
5. Chu, L.; Huang, C.; Liu, Q.; Cai, C.; Liu, G. Spatial Heterogeneity of Winter Wheat Yield and Its Determinants in the Yellow River Delta, China. *Sustainability* **2020**, *12*, 135. [\[CrossRef\]](#)
6. Liu, Y.; Song, H.; An, Z.; Sun, C.; Trouet, V.; Cai, Q.; Liu, R.; Leavitt, S.W.; Song, Y.; Li, Q.; et al. Recent anthropogenic curtailing of Yellow River runoff and sediment load is unprecedented over the past 500 y. *Proc. Natl. Acad. Sci. USA* **2020**, *117*, 18251–18257. [\[CrossRef\]](#)
7. Wang, R.; Huston, S.; Li, Y.; Ma, H.; Peng, Y.; Ding, L. Temporal Stability of Groundwater Depth in the Contemporary Yellow River Delta, Eastern China. *Sustainability* **2018**, *10*, 2224. [\[CrossRef\]](#)
8. Yi, L.; Chen, S.; Ortiz, J.D.; Chen, G.; Peng, J.; Liu, F.; Chen, Y.; Deng, C. 1500-year cycle dominated Holocene dynamics of the Yellow River delta, China. *Holocene* **2016**, *26*, 222–234. [\[CrossRef\]](#)
9. IOCAS. *Bohai Sea Geology*; Science Press: Beijing, China, 1985; p. 232. (In Chinese)
10. Xue, C.; Zhu, Z.; Lin, H. Holocene sedimentary sequence, foraminifera and ostracoda in west coastal lowland of Bohai Sea, China. *Quat. Sci. Rev.* **1995**, *14*, 521–530. [\[CrossRef\]](#)
11. Xue, C. Historical changes in the Yellow River delta, China. *Mar. Geol.* **1993**, *113*, 321–330. [\[CrossRef\]](#)
12. Liu, J.; Saito, Y.; Kong, X.; Wang, H.; Xiang, L.; Wen, C.; Nakashima, R. Sedimentary record of environmental evolution off the Yangtze River estuary, East China Sea, during the last ~13,000 years, with special reference to the influence of the Yellow River on the Yangtze River delta during the last 600 years. *Quat. Sci. Rev.* **2010**, *29*, 2424–2438. [\[CrossRef\]](#)
13. Saito, Y.; Wei, H.; Zhou, Y.; Nishimura, A.; Sato, Y.; Yokota, S. Delta progradation and chenier formation in the Huanghe (Yellow River) delta, China. *J. Asian Earth Sci.* **2000**, *18*, 489–497. [\[CrossRef\]](#)
14. Ren, R.; Chen, S.; Dong, P.; Liu, F. Spatial and Temporal Variations in Grain Size of Surface Sediments in the Littoral Area of Yellow River Delta. *J. Coast. Res.* **2012**, *28*, 44–53. [\[CrossRef\]](#)
15. Xue, C.T.; Cheng, G.D. Shelly ridges in west coast of Bohai Sea and Holocene Yellow River Delta system. In *Quaternary Processes and Events in China Offshore and Onshore Areas*; Yang, Z., Lin, H., Eds.; China Ocean Press: Beijing, China, 1989; pp. 117–125. (In Chinese)
16. Boyd, R.; Dalrymple, R.; Zaitlin, B. Classification of clastic coastal depositional environments. *Sediment. Geol.* **1992**, *80*, 139–150. [\[CrossRef\]](#)
17. Hori, K.; Saito, Y. An early Holocene sea-level jump and delta initiation. *Geophys. Res. Lett.* **2007**, *34*, 18401. [\[CrossRef\]](#)
18. Wu, X.; Bi, N.; Syvitski, J.; Saito, Y.; Xu, J.; Nitttrouer, J.A.; Bianchi, T.S.; Yang, Z.; Wang, H. Can Reservoir Regulation Along the Yellow River Be a Sustainable Way to Save a Sinking Delta? *Earth's Future* **2020**, *8*. [\[CrossRef\]](#)
19. Nicholls, R.J.; Cazenave, A. Sea-Level Rise and Its Impact on Coastal Zones. *Science* **2010**, *328*, 1517–1520. [\[CrossRef\]](#)
20. Syvitski, J.P.M.; Kettner, A.J.; Overeem, I.; Hutton, E.W.H.; Hannon, M.T.; Brakenridge, G.R.; Day, J.W.; Vorosmarty, C.J.; Saito, Y.; Giosan, L.; et al. Sinking deltas due to human activities. *Nat. Geosci.* **2009**, *2*, 681–686. [\[CrossRef\]](#)
21. Maroukian, H.; Karymbalis, E. Geomorphic evolution of the fan delta of the Evros river in western Greece and human impacts in the last 150 years. *Z. Geomorphol.* **2004**, *48*, 201–217. [\[CrossRef\]](#)
22. Karymbalis, E.; Valkanou, K.; Tsoudoulos, I.; Iliopoulos, G.; Tsanakas, K.; Batzakis, D.-V.; Tsironis, G.; Gallousi, C.; Stamoulis, K.; Ioannides, K. Geomorphic Evolution of the Lila River Fan Delta (Central Evia Island, Greece). *Geoscience* **2018**, *8*, 361. [\[CrossRef\]](#)
23. Brückner, H.; Vött, A.; Schriever, A.; Handl, M. Holocene delta progradation in the eastern Mediterranean—case studies in their historical context. *Mediterranean Eacute* **2005**, *104*, 95–106. [\[CrossRef\]](#)
24. Simeoni, U.; Corbau, C. A review of the Delta Po evolution (Italy) related to climatic changes and human impacts. *Geomorphology* **2009**, *107*, 64–71. [\[CrossRef\]](#)
25. Kranck, K.; Smith, P.C.; Milligan, T.G. Grain-size characteristics of fine-grained unflocculated sediments I: ‘one-round’ distributions. *Sedimentology* **1996**, *43*, 589–596. [\[CrossRef\]](#)
26. Kranck, K.; Smith, P.C.; Milligan, T.G. Grain-size characteristics of fine-grained unflocculated sediments II: ‘multi-round’ distributions. *Sedimentology* **1996**, *43*, 597–606. [\[CrossRef\]](#)

27. Pässe, T. Grain size distribution expressed as tanh-functions. *Sedimentology* **1997**, *44*, 1011–1014. [[CrossRef](#)]
28. Qin, X.; Cai, B.; Liu, T. Loess record of the aerodynamic environment in the east Asia monsoon area since 60,000 years before present. *J. Geophys. Res. Space Phys.* **2005**, *110*, B01204. [[CrossRef](#)]
29. Yi, L.; Yu, H.-J.; Ortiz, J.D.; Xu, X.-Y.; Chen, S.-L.; Ge, J.-Y.; Hao, Q.-Z.; Yao, J.; Shi, X.-F.; Peng, S.-Z. Late Quaternary linkage of sedimentary records to three astronomical rhythms and the Asian monsoon, inferred from a coastal borehole in the south Bohai Sea, China. *Palaeogeogr. Palaeoclim. Palaeoecol.* **2012**, *329–330*, 101–117. [[CrossRef](#)]
30. Sun, D.; Bloemendal, J.; Rea, D.; Vandenberghe, J.; Jiang, F.; An, Z.; Su, R. Grain-size distribution function of polymodal sediments in hydraulic and aeolian environments, and numerical partitioning of the sedimentary components. *Sediment. Geol.* **2002**, *152*, 263–277. [[CrossRef](#)]
31. Ashley, G.M. Interpretation of Polymodal Sediments. *J. Geol.* **1978**, *86*, 411–421. [[CrossRef](#)]
32. Passega, R. Texture as Characteristic of Clastic Deposition. *AAPG Bull.* **1957**, *41*, 1952–1984. [[CrossRef](#)]
33. Passega, R. Grain size representation by CM patterns as a geologic tool. *J. Sediment. Res.* **1964**, *34*, 830–847. [[CrossRef](#)]
34. Lyu, W.; Yang, J.; Fu, T.; Chen, Y.; Hu, Z.; Tang, Y.Z.; Lan, J.; Chen, G.; Su, Q.; Xu, X.; et al. Asian monsoon and oceanic circulation paced sedimentary evolution over the past 1,500 years in the central mud area of the Bohai Sea, China. *Geol. J.* **2020**, *55*, 5606–5618. [[CrossRef](#)]
35. Li, Y.; Yu, H.; Yi, L.; Su, Q.; Hu, K.; Xu, X.; Wang, J. Grain-size characteristics and its sedimentary significance of coastal sediments of the borehole Lz908 in the south Bohai Sea (the Laizhou Bay), China. *Mar. Sci.* **2014**, *38*, 107–113. (In Chinese) [[CrossRef](#)]
36. Zhang, L.; Chen, S.; Pan, S.; Yi, L.; Jiang, C. Sediment variability and transport in the littoral area of the abandoned Yellow River Delta, northern Jiangsu. *J. Geogr. Sci.* **2014**, *24*, 717–730. [[CrossRef](#)]
37. Kleinbaum, D.; Kupper, L.; Muller, K.; Nizam, A. *Applied Regression Analysis and Other Multivariable Methods*, 3rd ed.; Duxbury Press: Pacific Grove, CA, USA, 1997; p. 816.
38. Galloway, W.E. Process Framework for Describing the Morphologic and Stratigraphic Evolution of Deltaic Depositional Systems. In *Deltas: Models for Exploration*; Broussard, M.L., Ed.; Houston Geological Society: Houston, TX, USA, 1975; pp. 87–98.
39. Xu, J.S. Changes of sea level and chenier along Huanghua beach of the Bohai Bay. *Acta Oceanol. Sin.* **1994**, *13*, 68–77. (In Chinese)
40. Zhao, X.T.; Geng, X.S.; Zhang, J.W. Sea level changes of the eastern China during the past 20,000 years. *Acta Oceanol. Sin.* **1979**, *1*, 269–281. (In Chinese)
41. Stanley, D.J.; Warne, A.G. Worldwide Initiation of Holocene Marine Deltas by Deceleration of Sea-Level Rise. *Science* **1994**, *265*, 228–231. [[CrossRef](#)]
42. Milliman, J.D.; Yun-Shan, Q.; Mei-E, R.; Saito, Y. Man's Influence on the Erosion and Transport of Sediment by Asian Rivers: The Yellow River (Huanghe) Example. *J. Geol.* **1987**, *95*, 751–762. [[CrossRef](#)]
43. Mei-E, R.; Xianmo, Z. Anthropogenic influences on changes in the sediment load of the Yellow River, China, during the Holocene. *Holocene* **1994**, *4*, 314–320. [[CrossRef](#)]
44. Saito, Y.; Yang, Z.; Hori, K. The Huanghe (Yellow River) and Changjiang (Yangtze River) deltas: A review on their characteristics, evolution and sediment discharge during the Holocene. *Geomorphology* **2001**, *41*, 219–231. [[CrossRef](#)]
45. Chen, G.; Yi, L.; Chen, S.; Huang, H.; Liu, Y.; Xu, Y.; Cao, J. Partitioning of grain-size components of estuarine sediments and implications for sediment transport in southwestern Laizhou Bay, China. *Chin. J. Oceanol. Limnol.* **2013**, *31*, 895–906. [[CrossRef](#)]
46. Su, Q.; Peng, C.; Yi, L.; Huang, H.; Liu, Y.; Xu, X.; Chen, G.; Yu, H. An improved method of sediment grain size trend analysis in the Xiaoqinghe Estuary, southwestern Laizhou Bay, China. *Environ. Earth Sci.* **2016**, *75*. [[CrossRef](#)]
47. Fagherazzi, S. Self-organization of tidal deltas. *Proc. Natl. Acad. Sci. USA* **2008**, *105*, 18692–18695. [[CrossRef](#)]
48. Liu, T. *Loess and the Environment*; Ocean Press: Beijing, China, 1985; p. 174. (In Chinese)
49. Liu, T. *Loess and Arid Environment*; Anhui Science & Technology Press: Hefei, China, 2009; p. 537. (In Chinese)
50. Wang, Y.; Cheng, H.; Edwards, R.L.; He, Y.; Kong, X.; An, Z.; Wu, J.; Kelly, M.J.; Dykoski, C.A.; Li, X. The Holocene Asian Monsoon: Links to Solar Changes and North Atlantic Climate. *Science* **2005**, *308*, 854–857. [[CrossRef](#)] [[PubMed](#)]
51. Steinhilber, F.; Beer, J.; Fröhlich, C. Total solar irradiance during the Holocene. *Geophys. Res. Lett.* **2009**, *36*. [[CrossRef](#)]
52. Bond, G.; Kromer, B.; Beer, J.; Muscheler, R.; Evans, M.N.; Showers, W.; Hoffmann, S.; Lotti-Bond, R.; Hajdas, I.; Bonani, G. Persistent Solar Influence on North Atlantic Climate During the Holocene. *Science* **2001**, *294*, 2130–2136. [[CrossRef](#)]
53. Tan, L.; Cai, Y.; Yi, L.; An, Z.; Ai, L. Precipitation variations of Longxi, northeast margin of Tibetan Plateau since AD 960 and their relationship with solar activity. *Clim. Past* **2008**, *4*, 19–28. [[CrossRef](#)]
54. Jian, Z.; Wang, P.; Saito, Y.; Wang, J.; Pflaumann, U.; Oba, T.; Cheng, X. Holocene variability of the Kuroshio Current in the Okinawa Trough, northwestern Pacific Ocean. *Earth Planet. Sci. Lett.* **2000**, *184*, 305–319. [[CrossRef](#)]